Adiabatic Laminar Boundary-Layer/Shock-Wave Interactions on Flared Axisymmetric Bodies

HARRY P. HORTON*
von Kármán Institute for Fluid Dynamics, Rhode-Saint-Genèse, Belgium

A method is described for calculating the over-all properties of flare-induced laminar boundary-layer/shock-wave interactions on axisymmetric bodies at zero incidence in supersonic flow, under adiabatic conditions. The method consists of an extension to axisymmetric flow of the two-dimensional integral method of Lees and Reeves, as recently improved by Klineberg. The relationship between the local slope and Mach number of the external inviscid stream is calculated by a suitable inversion of the second-order shock-expansion method of Syvertson and Dennis. Satisfactory agreement is demonstrated between the theory and measurements on hollow cylinder-flare models at Mach numbers of 2.2 and 4.0.

Nomenclature

a = velocity profile parameter, Eq. (10); also speed of sound
$A_2 \ldots A_8$ = functions of a, Eq. (20)
B = $\gamma p M_e^2/2(M_e^2 - 1)$
C = $(\mu/\mu_\infty)/(T/T_\infty)$, Chapman-Rubesin parameter
D = determinant of Eqs. (17a–17c)
f = $2\mathcal{K} + [(3\gamma - 1)/(\gamma - 1)] + [(\gamma + 1)/(\gamma - 1)][m_e/(1 + m_e)]\mathcal{K} + (j)[(M_e^2 - 1)/m_e(1 + m_e)]Z$
F = $\mathcal{K} + (1 + m_e)/m_e$
h = $(R_{\delta_i}*/C)(M_e/M_\infty)[(1 + m_e)/m_e(1 + m_\infty)]$ tan Θ
$\mathcal{K}$ = θ_i/δ_i*
J = θ_i*/δ_i*
j = integer; 0 for displacement surface coupling, 1 for Crocco-Lees coupling
K = $(\beta C/R_{\delta_i}*)(M_\infty/M_e)$
L_1,L_2,L_3 = functions defined in Eqs. (19)
L = length of hollow cylindrical portion of body
m = $(\gamma - 1)M^2/2$
M = u/a, Mach number
N_1,N_2,N_3 = functions defined in Eqs. (19)
p = static pressure
P = $[\partial(U/U_e)/\partial(Y/\delta_i*)]_w$, skin friction parameter
Q = $\delta_i*d(\ln r_w)/ds$, divergence parameter
r = radial distance from body axis
r_c = radius of cylindrical portion of body
r_w = local radius of body
$r_{\delta}*$ = local radius of displacement surface
R = $(2\delta_i*/U_e^2)\int_0^{\delta_i}(\partial U/\partial Y)^2 dY$, dissipation parameter; also gas constant in Eq. (4)
R_u = $\rho_\infty u_\infty/\mu_\infty$, unit Reynolds number
$R_{\delta_i}*$ = $\delta_i* \cdot R_u$, Reynolds number
R_{r_c} = $r_c \cdot R_u$, Reynolds number
R_L = $L \cdot R_u$, Reynolds number
R_x = $x \cdot R_u$, Reynolds number
s = ordinate along body surface
T = static temperature
u,v = velocity components in (s,y) directions
U = transformed u component of velocity, Eq. (6)
x = ordinate along body axis
y = ordinate normal to body surface
Y = transformed ordinate normal to surface, Eq. (6)
Z = $(\delta_i - \delta_i*)/\delta_i*$
α = $\sin^{-1}(dr_w/ds)$, inclination of body surface to axis
β = $(a_e p_e)/(a_\infty p_\infty)$
γ = ratio of specific heats of gas
δ = flare or ramp angle; also boundary-layer thickness
$\delta*$ = displacement thickness, Eq. (12)
δ_i* = transformed displacement thickness, Eq. (9)
Δs = integration step length
ϵ = perturbation parameter
η = exponent, Eq. (24)
θ_i = $\int_0^{\delta_i}(U/U_e)[1 - (U/U_e)]dY$, tranformed momentum thickness
θ_i* = $\int_0^{\delta_i}(U/U_e)[1 - (U^2/U_e^2)]dY$, transformed mechanical energy thickness
Θ = inclination of displacement surface to body surface
μ = viscosity coefficient
$\nu(M)$ = Prandtl-Meyer angle
ρ = gas density
ϕ = inclination of displacement surface to body axis
Ω = function of Mach number, Eq. (22)

Subscripts

a,b,c,d = successive points in numerical integration
e = local conditions in external stream
i = transformed quantity in Stewartson plane
TC = on tangential cone-frustum
w = at body surface
0 = beginning of interaction
∞ = undisturbed freestream conditions

Received June 29, 1970; revision received April 5, 1971. The work was carried out while the author was in receipt of a fellowship under the European Programme of the Royal Society of London, in conjunction with the Fonds National de la Recherche Scientifique of Belgium. The author gratefully acknowledges the guidance of J. J. Ginoux, who suggested this research. Thanks are also due to M. Riethmuller for his assistance in developing the computer program and to R. Leblanc for advance access to his experimental data.

Index categories: Jets, Wakes, and Viscid-Inviscid Flow Interactions; Supersonic and Hypersonic Flow; Boundary Layers and Convective Heat Transfer—Laminar.

* Assistant Professor.

I. Introduction

THE interaction between a two-dimensional laminar boundary layer and a shock wave, either incident upon the surface or generated by a rapid change of surface slope, has been the subject of a large number of investigations, both experimental[1–4] and analytical.[5–9]

Similar interactions may occur on axisymmetric bodies in situations of practical importance, for example on missiles and space vehicles with flared bases, and a number of experimental studies have been made.[10–13] In experimental work, axisymmetric models have the advantage, as compared with planar models, that they do not suffer from finite-aspect-ratio effects. Such models, spun rapidly about their axes, have been used by Leblanc and Ginoux[14] in the current von Kármán Institute (VKI) research on the effect of small cross

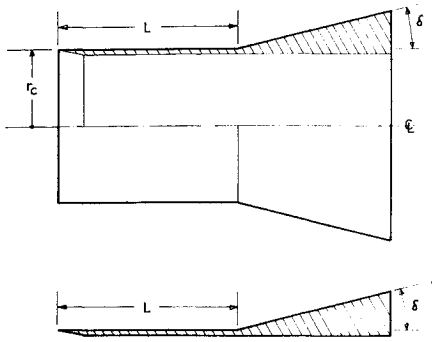

Fig. 1 Hollow cylinder-flare configuration, with planar counterpart.

flow upon shock-induced laminar separation. Accurate pressure measurements have also been made on these models with negligibly small rates of spin.

In the absence of adequate existing theories, the method described herein was developed to predict the over-all flow properties, such as the pressure and boundary-layer thickness distributions, of interactions on flared axisymmetric bodies at zero incidence, without spin, for comparison with the VKI measurements. The method is, however, of more general interest. A later paper will deal with the case of spinning bodies.

The two-dimensional integral method of Lees and Reeves,[6] in the improved form of Klineberg,[15,9] was chosen as the basis of the present method, because this approach is of greater simplicity than, but of comparable accuracy with, alternative procedures such as those of Refs. 7 and 8.

In its present form, the method is applicable to the adiabatic wall case only, but the extension to nonadiabatic conditions would be straightforward, the two-dimensional theory of Klineberg again providing a suitable basis. Furthermore, we consider only the hollow cylinder-flare configuration, shown in Fig. 1, this being the axisymmetric equivalent of the widely studied planar ramped flat plate. However, closed-nose bodies could also be treated, either by using conventional boundary-layer methods upstream of the start of the flare-induced interaction or, more accurately, by using the equations derived herein to calculate the self-induced interaction in the upstream region.

The differences in the pressure distributions between flows over a planar ramp and an axisymmetric flare at $M_\infty = 2.2$, in both the inviscid (theoretical) and viscous (measured) cases, are shown in Fig. 2. In inviscid flow, there is a marked overcompression on the flare, as opposed to the constant pressure on the ramp, whereas in the viscous case the upstream influence is appreciably less in the axisymmetric case than in the planar, and the over-all pressures are generally reduced.

Supersonic interactive calculations require the solution of both the boundary layer and the inviscid outer stream. In axisymmetric flow, the effects of streamline convergence upon both of these flow components must be considered. For example, the drop in pressure along the flare in inviscid flow, shown in Fig. 2, is due to external streamline convergence, and a comparable drop occurs in the viscous case. It will be shown in Sec. II.E that external stream convergence has a more important effect upon flare-induced interactions than does the boundary-layer convergence. Hence the only previous analyses of axisymmetric laminar interactions known to the author, those of Nielsen et al.,[16,26,27] are inadequate insofar as a two-dimensional external flow relation was used.

The present method, in addition to including boundary-layer convergence effects, takes external flow convergence into account by using a suitably inverted form of the second-order shock-expansion method of Syvertson and Dennis.[17] This method, which is simple yet accurate, could also be used in conjunction with alternative procedures for calculating the boundary-layer development, such as the finite-difference method of Reyhner and Flügge-Lotz.[8] The use of the axisymmetric method of characteristics was not considered to be practicable, because of the large computing time required.

The system of equations to be solved is developed in Sec. II, and the method of solution, together with the appropriate boundary conditions, is discussed in Sec. III. Comparisons between predictions of the theory and measurements are given in Sec. IV, and a discussion of the range of application of the theory is given in Sec. V.

II. Analysis

A. Basic Viscous Flow Equations

We assume, as is usual in the two-dimensional case, that the boundary-layer approximation provides an adequate description of both the attached and separated viscous flow regions. We further assume a perfect gas with constant ratio of specific heats, that there is zero heat transfer at the surface, that the Prandtl number is equal to unity, and that the boundary-layer thickness δ is small compared to the local body radius r_w. The latter assumption, which neglects transverse curvature effects, is examined in Ref. 18, where it is shown that the resulting errors are negligible when the maximum value of δ/r_w is at least 8%. This condition is satisfied in the experiments considered here.

Then, in orthogonal coordinates (s,y) measured along and normal to the body surface, the equations of longitudinal and normal momentum, continuity and state, for flow in the laminar boundary over an axisymmetric body at zero incidence and without rotation, are

$$\rho\left(u\frac{\partial u}{\partial s} + v\frac{\partial u}{\partial y}\right) = -\frac{\partial p}{\partial s} + \frac{\partial}{\partial y}\left(\mu\frac{\partial u}{\partial y}\right) \tag{1}$$

$$0 = \partial p/\partial y \tag{2}$$

$$(\partial/\partial s)(\rho u r_w) + r_w(\partial/\partial y)(\rho v) = 0 \tag{3}$$

$$p = \rho RT \tag{4}$$

The Busemann integral of the energy equation is used to relate temperature and velocity within the boundary layer, so that

$$T/T_e = 1 + m_e(1 - u^2/u_e^2) \tag{5}$$

B. Integral Equations

Following a similar procedure to that used in the two-dimensional case,[6,9] the partial differential boundary-layer equations may be integrated with respect to y to obtain the momentum integral and first moment of momentum equations. After the application of a slightly modified Stewart-

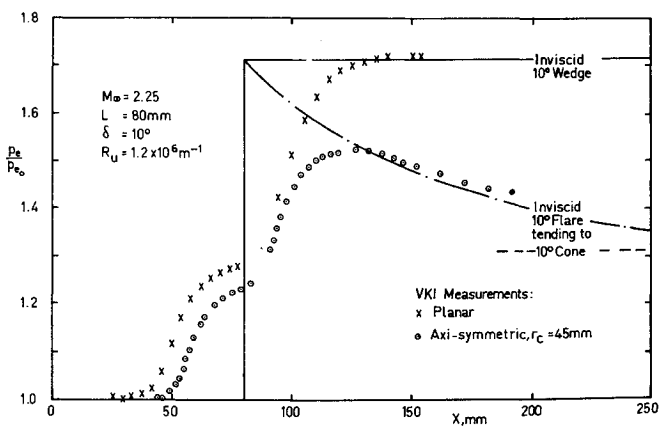

Fig. 2 Comparison between planar and axisymmetric flows.

son[19] scaling

$$Y = \frac{a_e}{a_\infty}\int_0^y \frac{\rho}{\rho_\infty}\,dy \qquad U = \frac{a_\infty}{a_e}\,u \tag{6}$$

we obtain the following pair of equations in transformed variables:

$$\mathfrak{K}\frac{d\delta_i^*}{ds} + \delta_i^*\frac{d\mathfrak{K}}{ds} + (2\mathfrak{K}+1)\frac{\delta_i^*}{M_e}\frac{dM_e}{ds} = \frac{\beta C}{R_{\delta_i^*}}\frac{M_\infty}{M_e}P - \mathfrak{K}\frac{\delta_i^*}{r_w}\frac{dr_w}{ds} \tag{7}$$

$$J\frac{d\delta_i^*}{ds} + \delta_i^*\frac{dJ}{ds} + 3J\frac{\delta_i^*}{M_e}\frac{dM_e}{ds} = \frac{\beta C}{R_{\delta_i^*}}\frac{M_\infty}{M_e}R - J\frac{\delta_i^*}{r_w}\frac{dr_w}{ds} \tag{8}$$

where δ_i^* is the transformed displacement thickness given by

$$\delta_i^* = \int_0^{\delta_i}[1 - (U/U_e)]\,dY \tag{9}$$

and the other variables are defined in the Nomenclature.

Equations (7) and (8) may be used to obtain an approximate solution of the boundary layer by assuming a suitable profile family. Now these equations may be reduced to two-dimensional form by means of the Mangler[20] transformation, under which the streamwise velocity is invariant and the y ordinate linearly scaled. Thus, although it is convenient to retain the equations in axisymmetric form, the profile family used in two-dimensional calculations[9] may be used. We therefore adopt the Lees-Reeves[6] profile parameter a, defined as

$$a = [\partial(U/U_e)/\partial(Y/\delta_i)]_{Y=0} \qquad \text{for attached flow} \tag{10a}$$

$$a = (Y/\delta_i)_{U/U_e=0} \qquad \text{for separated flow} \tag{10b}$$

The quantities $\mathfrak{K}$, J, P, and R are assumed to be functions of a only, and polynomial representations of these quantities, as well as of $d\mathfrak{K}/da$ and $dJ/d\mathfrak{K}$, have been computed by Klineberg[9] from attached and reversed flow similar solutions of the boundary-layer equations.

C. Coupling of the Viscous and Inviscid Flows

Interactive calculations are carried out by integrating the boundary-layer integral equations simultaneously with a coupling equation, relating the slope of the inviscid stream induced by the growth of the boundary layer to that dictated by the outer inviscid flow relations.

From the definition of displacement thickness, the effective radius r_{δ^*} of the body of revolution which would have the same pressure distribution in inviscid flow as the real body in viscous flow is

$$r_{\delta^*} = r_w + \delta^*\cos\alpha \tag{11}$$

where δ^* is the displacement thickness defined by

$$\delta^* = \int_0^{\delta}[1 - (\rho u/\rho_e u_e)]\,dy \tag{12}$$

and

$$\alpha = \sin^{-1}(dr_w/ds) \tag{13}$$

Differentiation of Eq. (11) with respect to s leads to the coupling equation

$$d\delta^*/ds = \tan(\phi - \alpha) \equiv \tan\Theta \tag{14}$$

The inclination Θ of the equivalent inviscid stream to the surface is a function of the upstream geometry of the effective surface, as well as the local Mach number, as will be discussed in Sec. II.E.

This coupling equation differs somewhat from that used by Lees and Reeves,[6] who, following Crocco and Lees,[5] evaluate the slope of the inviscid flow by equating it to the slope of the streamline at the outer boundary-layer edge. This leads, in the axisymmetric case, to a coupling equation of the form

$$(d\delta^*/ds) - (\delta - \delta^*)(d/ds)\ln(\rho_e u_e r_w) = \tan\Theta \tag{15}$$

The additional term is of arbitrary magnitude because the boundary-layer thickness δ is not a well-defined quantity, and we therefore prefer the displacement surface coupling, which has been used by other previous authors, for example, in Refs. 7 and 8, and which does not involve this arbitrariness. A comparison in Sec. IV.B between calculations made using the alternative methods of coupling shows the difference to be small in any case.

Application of the Stewartson scalings to Eqs. (14) or (15) results in

$$F\frac{d\delta_i^*}{ds} + \delta_i^*\frac{d\mathfrak{K}}{ds} + f\frac{\delta_i^*}{M_e}\frac{dM_e}{ds} = \frac{\beta C}{R_{\delta_i^*}}\frac{M_\infty}{M_e}h + (j)\frac{Z}{m_e}\frac{\delta_i^*}{r_w}\frac{dr_w}{ds} \tag{16}$$

where j is an integer having the value 0 or 1, depending on whether displacement surface [Eq. (14)] or Crocco-Lees [Eq. (15)] coupling is used, and other variables are defined in the Nomenclature. The profile parameter Z is given as a polynomial in a by Klineberg.[9]

D. Working Form of the Differential Equations

The two transformed ordinary differential equations for the boundary layer, Eqs. (7) and (8), together with the transformed coupling equation, Eq. (16), may be rearranged in the following form convenient for numerical integration:

$$\delta_i^* d(\ln M_e)/ds = (KN_1 + QL_1)/D \tag{17a}$$

$$d\delta_i^*/ds = (KN_2 + QL_2)/D \tag{17b}$$

$$\delta_i^* da/ds = (KN_3 + QL_3)/D \tag{17c}$$

where

$$K = \frac{\beta C}{R_{\delta_i^*}}\frac{M_\infty}{M_e} \qquad Q = \delta_i^*\frac{d(\ln r_w)}{ds} \tag{18}$$

and

$$\left.\begin{aligned} D &= A_6 + A_3 f - A_8 F \\ N_1 &= A_2 + A_3 h - A_4 F \\ N_2 &= A_7 + A_4 f - A_8 h \\ N_3 &= \frac{A_6 h - A_2 f - A_7 F}{d\mathfrak{K}/d_a} \\ L_1 &= A_3(F + jZ/m_e) \\ L_2 &= -(A_6 + A_3 f + jA_3 Z/m_e) \\ L_3 &= \frac{A_6(F + jZ/m_e)}{d\mathfrak{K}/da} \end{aligned}\right\} \tag{19}$$

The coefficients A_n are functions of the profile parameter a only and in terms of the integral quantities are

$$\left.\begin{aligned} A_2 &= (PJ - \mathfrak{K}R) \\ A_4 &= (PdJ/d\mathfrak{K} - R) \\ A_6 &= J(1 - \mathfrak{K}) \\ A_8 &= (2\mathfrak{K}+1)dJ/d\mathfrak{K} - 3J \\ A_3 &= (\mathfrak{K}dJ/d\mathfrak{K} - J) \\ A_5 &= 3J \\ A_7 &= (2\mathfrak{K}+1)R - 3PJ \end{aligned}\right\} \tag{20}$$

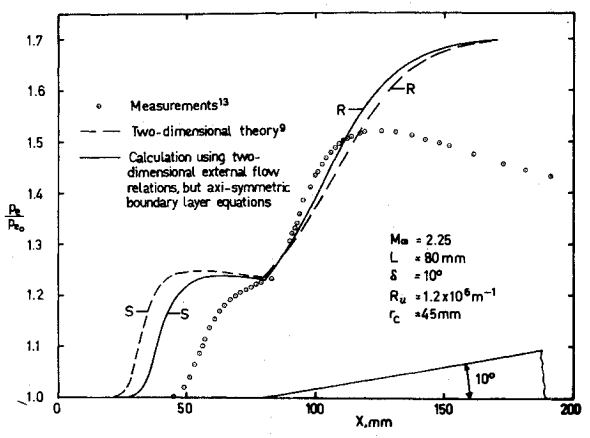

Fig. 3 Comparison between axisymmetric measurements and two-dimensional theory of Klineberg, without and with modification for boundary-layer convergence.

E. Calculation of the Inviscid Flow Inclination

In order to integrate Eqs. (17), it is necessary to compute Θ at each step by solving the inviscid outer flow. In two-dimensional flow, the Prandtl-Meyer relation is usually used at moderate supersonic speeds, but in axisymmetric flow there is no such simple relationship between slope and Mach number. As remarked in Sec. I, Nielsen et al.[16,26,27] use the Prandtl-Meyer relation for axisymmetric calculations with reasonable success at high Mach numbers, but this approximation can lead to very large errors at lower Mach numbers when used in conjunction with the present boundary-layer method, as Fig. 3 shows. This figure shows pressure measurements on an axisymmetric hollow cylinder-flare model, compared with two calculations based on the Klineberg[9] method, both using the Prandtl-Meyer external flow relations, but respectively with and without the inclusion of the boundary-layer convergence terms [QL_1,QL_2,QL_3 in Eqs. (17)]. It is evident that the correct qualitative behavior can be predicted only by also including convergence effects in the external flow, and it is reasonable to suppose that this conclusion is not dependent upon the particular method of boundary-layer calculation used.

The second-order shock-expansion method of Syvertson and Dennis[17] for calculating the pressure on a body of revolution takes account of such effects and may be easily inverted to calculate, for the present problem, the displacement surface slope in terms of the local Mach number M† and the upstream displacement surface geometry. The accuracy of the method for Mach numbers between 3 and 6 was demonstrated by the original authors, and in Ref. 18 it is shown that the accuracy is maintained at very low supersonic Mach numbers. A particular advantage of this method is that it yields, by its formulation, the correct cone pressure far downstream.

The present application of the method is as follows. Referring to Fig. 4, at each integration step of elemental length Δs, the displacement surface is approximated by a cone-frustum element of semiangle ϕ. At the slope discontinuity between each adjacent pair of elements, there is a Mach number discontinuity, as in the two-dimensional case, whereas along the length of an element the Mach number changes due to convergence effects. Each small discontinuity is considered isentropic and is furthermore locally two-dimensional, and so the Prandtl-Meyer relation is used at the discontinuities. The pressure variation along an element is calculated from an exponential curve fitted to the pressure gradient immediately behind the discontinuity and to the pressure that would exist on a cone of the same semiangle as the local cone-frustum.

† In this subsection, the suffix e is dropped, for brevity, since only the external flow is considered.

Referring again to Fig. 4, suppose that it is required to find the slope ϕ_c of the displacement surface at point c. The Mach numbers M_{a_2} and M_{b_1} before and after the discontinuity at the preceding point b are known, and the Mach number *after* the discontinuity at point c is calculated, for Eulerian integration, from

$$M_{c_1} = M_{b_1} + \Delta s(dM/ds)_b$$

where $(dM/ds)_b$ is determined from the boundary-layer calculation. (For Runge-Kutta integration, each substep is treated as a step.) The corresponding pressures follow from isentropic flow relations. The pressure gradient behind the discontinuity at point b is given in Ref. 17 to be

$$\left(\frac{\partial p}{\partial s}\right)_{b_1} = \frac{B_{b_1}}{r_{\delta b}*}\left(\frac{\Omega_{a_2}}{\Omega_{b_1}}\sin\phi_a - \sin\phi_b\right) + \frac{B_{b_1}}{B_{a_2}}\frac{\Omega_{a_2}}{\Omega_{b_1}}\left(\frac{\partial p}{\partial s}\right)_{a_2} \quad (21)$$

where

$$B = \frac{\gamma p M^2}{2(M^2-1)}$$
$$\Omega = \frac{1}{M}\left[\frac{1+\frac{1}{2}(\gamma-1)M^2}{\frac{1}{2}(\gamma+1)}\right]^{(\gamma+1)/2(\gamma-1)} \quad (22)$$

The pressure variation along the element bc is then given by[17]

$$p = p_{TC_b} - (p_{TC_b} - p_{b_1})\exp(-\eta) \quad (23)$$

where

$$\eta = \left(\frac{\partial p}{\partial s}\right)_{b_1}\left(\frac{s-s_b}{p_{TC_b}-p_{b_1}}\right) \quad (24)$$

and p_{TC} is the pressure at M_∞ on a cone of semiangle ϕ_b. In the present calculations, p_{TC} was evaluated using the second-order explicit formula of Van Dyke.[21]

The pressure p_{b_2} just ahead of point c is obtained by putting $s = s_c$ in Eqs. (23) and (24), and the corresponding Mach number M_{b_2} is calculated from the ientropic flow relations. Finally, ϕ_c is calculated by using the Prandtl-Meyer relation

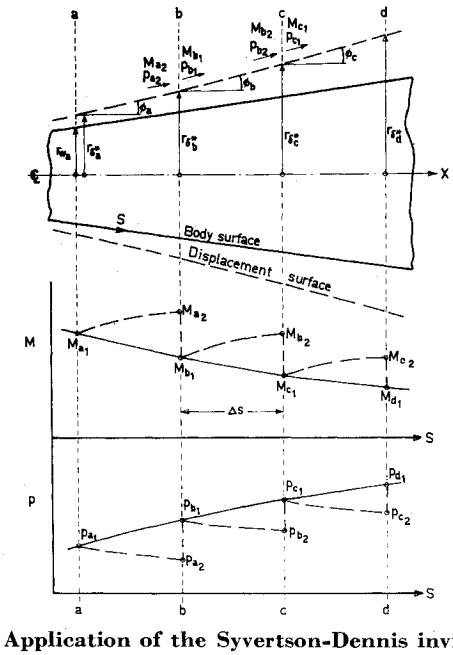

Fig. 4 Application of the Syvertson-Dennis inviscid flow method to the step-by-step calculation of axisymmetric interactive flows.

at the discontinuity, so that

$$\phi_c = \phi_b + \nu(M_{b_2}) - \nu(M_{c_1}) \tag{25}$$

and Θ_c follows from $\Theta_c = \phi_c - \alpha_c$.

The value of $(dp/ds)_{b_2}$ is required for the next step and is

$$(dp/ds)_{b_2} = (dp/ds)_{b_1} \exp(-\eta_c) \tag{26}$$

III. Solution Procedure

A. Nature of Solutions

Klineberg[15] has shown that self-induced viscous flow along a planar ramped flat plate is always subcritical in adiabatic flow, that is, upstream propagation of a disturbance occurs, and the governing equations are unstable. Now the axisymmetric hollow cylinder-flare configuration considered here is a direct analog of this planar case, and, since the expression for the determinant D, Eq. (19), whose vanishing marks the transition from a subcritical to a supercritical state, is identical for planar and axisymmetric flows, it follows that the axisymmetric flow is also subcritical.

B. Initial Conditions for the Numerical Integration

In the planar case, Klineberg[15] determines the initial values of M_e, δ_i^*, and a for the calculation of ramp-induced interactions from analytic expressions for self-induced flat-plate flow. Comparable analytic expressions cannot be obtained for the self-induced interaction on hollow axisymmetric cylinders, but numerical solutions may be calculated using Eqs. (17). Because of the leading-edge singularity, it is necessary to assume that two-dimensional conditions exist in this vicinity, and the analytic expressions of Klineberg are used to start the downstream numerical integration at a point close to the leading edge. It has been ascertained that the results are insensitive to the distance of this point from the leading edge, provided that it is small compared with the body radius. The interpolation procedure outlined in Sec. III.E may be used to suppress divergent solutions.

The results of such a calculation, with $M_\infty = 2.21$ and $R_{r_c} = 2 \times 10^5$, are compared with the two-dimensional solution in Fig. 5. The difference is small. Also included are measurements from Ref. 14 for values of R_{r_c} about 2×10^5, but the scatter is too great to allow conclusions to be drawn concerning the possible improvement resulting from the inclusion of axisymmetric effects in the calculation.

For convenience, the flare-induced interaction calculations presented here were therefore carried out using the two-dimensional analytic solutions for the self-induced interaction as initial conditions. The resulting inaccuracies are certainly small, because the self-induced pressures are not large. This was verified by means of a test calculation for the case to be presented in Fig. 7c, using axisymmetric initial values calculated as described previously. The results differed only insignificantly from those of a calculation using two-dimensional initial conditions. At higher Mach numbers, when self-induced pressures are more important, the effect of axisymmetry

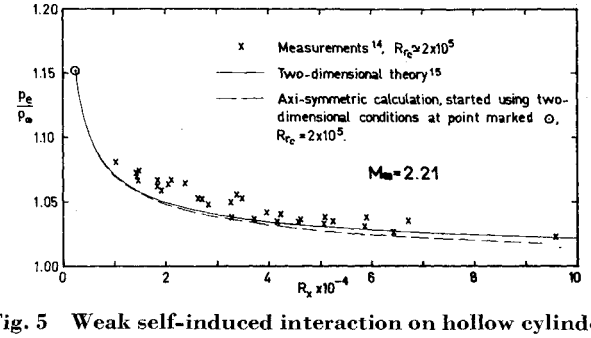

Fig. 5 Weak self-induced interaction on hollow cylinders.

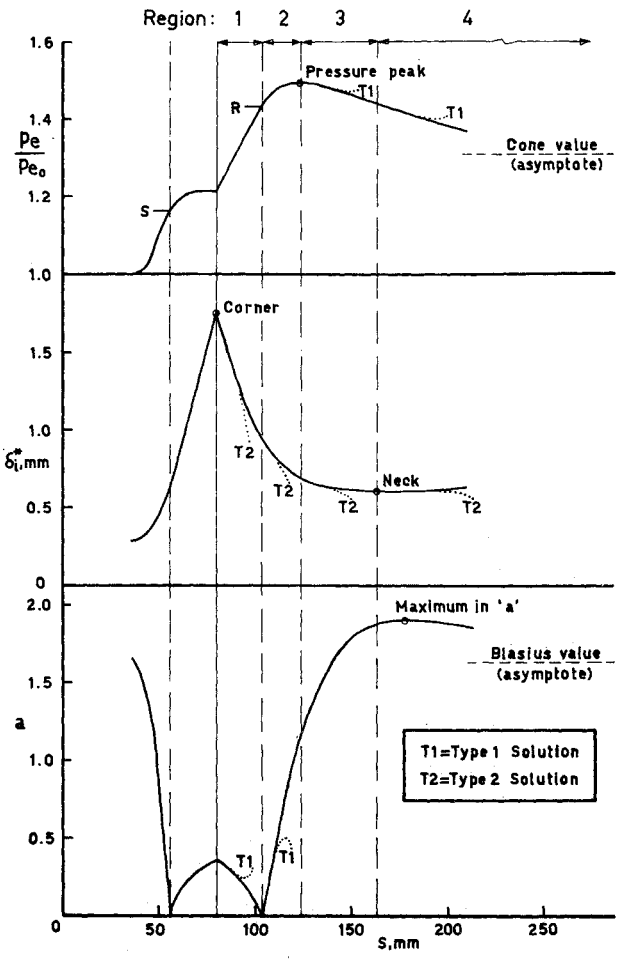

Fig. 6 Behavior of solutions and tests for divergence.

upon the external flow is reduced, and the two-dimensional relations should still provide suitable initial values.

The main interaction is generated by using initial conditions generated by applying a small perturbation ϵ at a point s_0 to the analytic self-induced interaction expansions for M_e, δ_i^*, and a in a consistent manner.[22,15] In accordance with the assumption that the flow upstream of s_0 is two-dimensional, the value of the pressure gradient $(\partial p/\partial s)_{a_2}$ in Eq. (21) is taken to be zero at s_0, and the Prandtl-Meyer relation is used to determine ϕ at this point.

The values of ϵ and s_0 are iterated in order to satisfy the downstream boundary conditions described in Sec. III.D. However, the same solutions can be obtained by using different combinations of ϵ and s_0,[22] and so in practice it is not necessary to iterate both quantities.

C. Conditions at the Corner

From physical considerations, the inclination ϕ of the displacement surface to the body axis must be continuous. Since α changes discontinuously at the corner from zero to the flare angle δ, and $\Theta = \phi - \alpha$, we have that Θ changes at the corner by $(-\delta)$. The derivatives with respect to s of M_e, δ_i^*, and a are then discontinuous at the corner, since they depend on Θ.

D. Downstream Boundary Conditions

Of the infinity of solutions which may be generated by varying ϵ and s_0, the required one is that which tends smoothly to self-preserving cone flow at downstream infinity. Adjacent solutions follow the required solution for some distance but then rapidly diverge toward a new compression (type 1) or an expansion (type 2). Values of ϵ and s_0 which are too

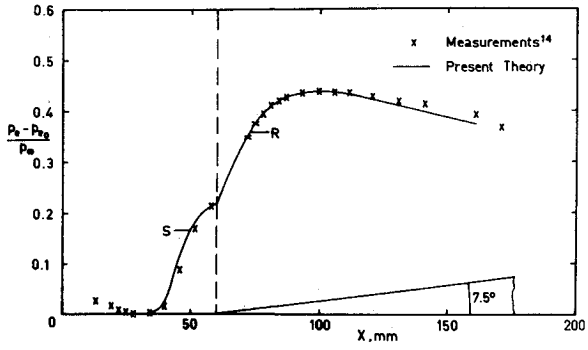

a) L = 60 mm, R_u = 1.47 × 10⁶ m⁻¹, δ = 7.5°

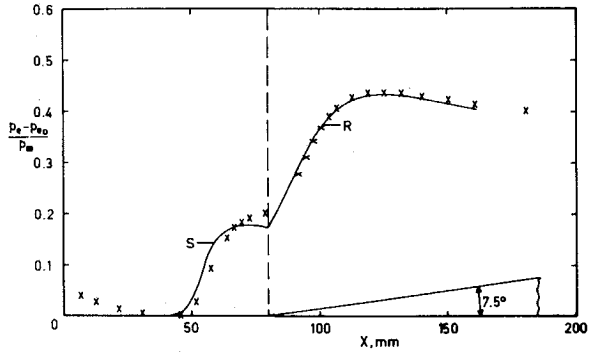

b) L = 80 mm, R_u = 2.65 × 10⁶ m⁻¹, δ = 7.5°

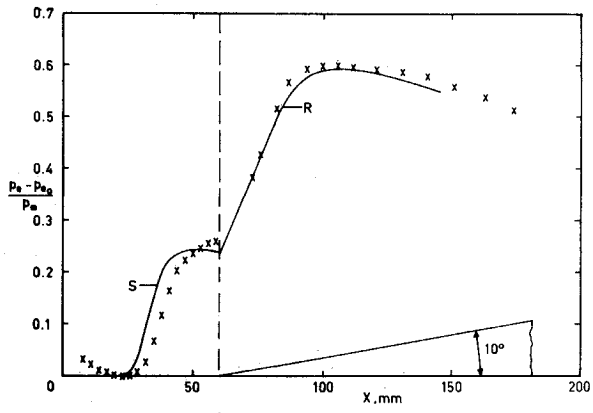

c) L = 60 mm, R_u = 1.47 × 10⁶ m⁻¹, δ = 10.0°

Fig. 7 Comparison between present theory and measurements on the 100-mm-radius VKI model at M_∞ = 2.21.

small produce type 1 solutions, and vice versa. After the corner, the following tests are used to determine the type of divergence (see Fig. 6):

Region 1: from corner to reattachment point: $da/ds > 0$ indicates type 1; $d\Theta/ds < 0$ indicates type 2.

Region 2: from reattachment to pressure peak: $da/ds < 0$ indicates type 1; $d\Theta/ds < 0$ indicates type 2.

Region 3: from pressure peak to neck (minimum in δ_i^*): $dM_e/ds < 0$ indicates type 1; $d\Theta/ds < 0$ indicates type 2.

Region 4: downstream of neck: $dM_e/ds < 0$ indicates type 1; $d\delta_i^*/ds$ indicates type 2.

The test on $d\Theta/ds$ is, by Eq. (14), equivalent to a test on $d^2\delta^*/ds^2$; a change of its sign thus indicates an inflexion in the displacement surface such that it turns toward the body surface, which evidently indicates an expansion. The tests on dM_e/ds and da/ds are self-explantory. The type 2 test is changed to a test on $d\delta^*/ds$ in region 4 because the existence of an inflexion point in δ^* in the correct solution does not permit the test on $d\Theta/ds$; it is equally indicative of an expansion in this region. (This test could be replaced by $da/ds > 0$ downstream of the maximum in a.)

The properties of the required solution obtained through the use of these tests are that dM_e/ds and da/ds tend to zero far downstream, whereas M_e and a tend to the cone and Blasius values, respectively. Note that the overshoot in a results from the expansion following the pressure peak.

E. Interpolation Procedure

The precision to which ϵ and s_0 need be iterated may be considerably reduced by using an interpolation procedure as described in Refs. 15 and 23. After iterating to obtain two solutions of opposite type which do not begin to diverge appreciably until after reattachment, an average of all relevant quantities is made between the two solutions, at a point where the pressures first differ by more than a specified amount. These averages are used as initial conditions for a continuation of the solution. When this solution itself diverges, another interpolation is made between this and the previous solution of opposite type. This may be repeated to continue the solution as far as required.

F. Computation Details

The calculations described in the following section were carried out using an IBM 1130 computer, using fourth-order Runge-Kutta integration. The computer program was based on a FORTRAN program for the two-dimensional method of Klineberg, described and listed by Riethmuller and Ginoux.[23]

IV. Comparisons Between Theory and Experiment

A. VKI 100-mm-Radius Model Tests

Figures 7a–7c show a series of comparisons between the present theory and some careful measurements carried out by Leblanc and Ginoux[14] at the VKI at M_∞ = 2.21. In addition to being accurately aligned with the undisturbed flow, the hollow cylinder-flare model was slowly rotated about its axis, in order to average out residual errors from misalignment of the model and nonuniformity of the freestream. The pressures are presented in the form $(p_e - p_{e_0})/p_\infty$ used in Ref. 14.

The agreement between theory and experiment is excellent for the 7.5° flare at the lower value of R_L (Fig. 7a) and somewhat less good at the higher (Fig. 7b), whereas, for the 10° flare (Fig. 7c), a more marked disagreement occurs in the free-interaction region upstream of the corner. Since the extent of separated flow increases with increase of both R_L and flare angle, it appears that the theory becomes increasingly inaccurate as the length (or, probably more importantly, the maximum depth) of the separated region is increased. This may well be attributable to inadequacies in the basic Lees-Reeves-Klineberg method, rather than in the present extension to axisymmetric flow, since a similar divergence between theory and experiment occurs in planar flow. As mentioned in Sec. III.B, inaccuracies due to the use of two-dimensional initial conditions are insignificant.

In all three cases, the predicted pressure distributions on the flare are in good agreement with the measurements.

B. VKI 45-mm-Radius Model Tests

The second group of comparisons (Figs. 8a and 8b) is with some earlier VKI measurements[13] on a model similar to that discussed previously but of smaller radius. These tests were carried out before the need for extremely accurate alignment of the model was fully appreciated and are therefore not so reliable as the measurements on the larger model. The comparisons are, however, of interest because the axisymmetric effects, characterized by the radius-to-length ratio r_c/L, are

significantly greater than those on the larger model. The conventional presentation of pressures in the form p_e/p_{e_0} is used here, because p_∞ was not measured accurately.

Figure 8a shows a comparison for a 10° flare. The improvement in the theoretical prediction resulting from the inclusion of convergence effects in the external flow may be seen by comparison with Fig. 3. However, a discrepancy still exists between theory and measurement in the free-interaction region, similar to that observed for the larger-radius model with the 10° flare. Also, the theoretical pressure maximum is rather lower than that measured.

For a flare angle of 7.5° (Fig. 8b), the agreement between theory and experiment is excellent ahead of the separation point, but the predicted pressures are thereafter somewhat lower than those measured. More accurate experiments with models having small values of r_c/L are required to determine whether these discrepancies are due to experimental error or to inaccuracies in the theory. The possibility that transverse curvature effects, neglected in the theory by virtue of the assumption that δ/r_w is small, might be appreciable for this model is examined in Ref. 18, but it is shown that such effects are very small.

A calculation using Crocco-Lees coupling, Eq. (15), is also shown in Fig. 8b, for comparison with the calculation using displacement surface coupling, used in the remainder of the calculations. The difference is small, and, since the effect of the additional term in the coupling equation is near its maximum at this Mach number and reduces rapidly with increasing Mach number, it may be concluded that the differences arising from the use of the alternative coupling equations are not important.

C. JPL 127-mm-Radius Model Tests

The final comparison, shown in Fig. 9, is with measurements on a hollow cylinder-flare model, carried out by Lewis et al.[24] at $M_\infty = 4.0$ at the Jet Propulsion Laboratory. The

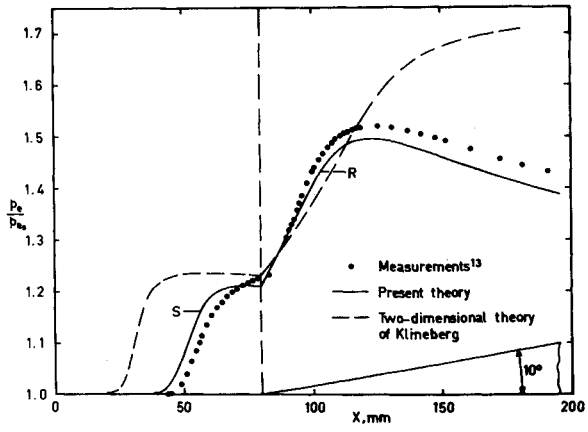

a) $L = 80$ mm, $R_u = 1.2 \times 10^6$ m^{-1}, $\delta = 10.0°$

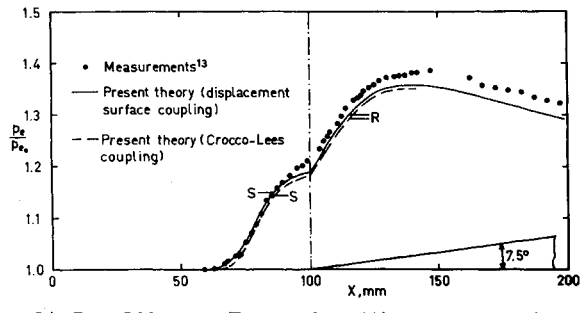

b) $L = 100$ mm, $R_u = 1.2 \times 10^6$ m^{-1}, $\delta = 7.5°$

Fig. 8 Comparisons between present theory and measurements on the 45-mm-radius VKI model at $M_\infty = 2.25$.

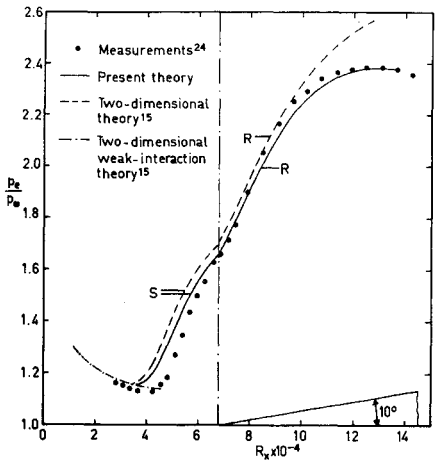

Fig. 9 Comparison between theory and measurements on the 127-mm-radius model of Lewis et al. at $M_\infty = 4.0$.

pressures are presented in the form p_e/p_∞, because a serious discrepancy can arise in the p_e/p_{e_0} representation, at Mach numbers high enough for the self-induced pressures to be appreciable before the start of the main interaction, if the theoretical and measured values of s_0 are not the same, as in this case.

The agreement between the axisymmetric theory and the measurements is very satisfactory on the flare. However, a discrepancy exists between theory and experiment in the free-interaction region, similar to that observed previously for the cases with 10° flare angles.

Also shown in Fig. 9 is a curve computed using the planar method of Klineberg. The difference between the axisymmetric and planar calculations is not so pronounced as at $M_\infty = 2.2$ but is still important.

The measurements in the self-induced interaction region are in good agreement with the planar weak-interaction solution of Klineberg,[15] also shown in Fig. 9.

V. Discussion

The foregoing comparisons indicate that the present inversion of the Syvertson-Dennis method is a reliable approximate means of determining the external flow in axisymmetric interactive calculations in the Mach number range from 2.2 to 4. It is shown in Ref. 18 that the method retains its accuracy at supersonic Mach numbers as low as 1.3, whereas the upper range of validity is governed by the condition[17] that $(M_\infty^2 - 1)^{1/2} \cdot \tan\delta$ should not be greater than about 2.5. For a 10° flare, this corresponds to an upper limit of $M_\infty \simeq 12$.

As in the planar case, certain basic assumptions of the present interaction theory become suspect at high Mach numbers. For example, pressure variations normal to the surface and entropy changes in the external stream, neglected in the theory, become appreciable. Furthermore, the adiabatic case is only of rather academic interest at high Mach numbers, because of the high temperatures involved.

It is hoped that the difference between theory and experiment in the free-interaction region, observed in the preceding section for cases with large separated regions, may be largely eliminated by improvements in the Lees-Reeves-Klineberg separated boundary-layer theory used as a basis for the present method. Such improvements are at present being investigated at VKI by M. L. Riethmuller.

Finally, we may observe that convergence effects in the external stream decrease in importance with increase of Mach number, so that the generalized shock-expansion method of Eggers and Savin[25] should yield acceptable results at high Mach numbers, since it amounts to the Syvertson-Dennis method without allowance for convergence.

VI. Conclusions

1) Boundary-layer convergence effects alone are insufficient to account for the large observed differences, in upstream influence and over-all pressure level, between supersonic laminar boundary-layer/shock-wave interactions on equivalent planar and axisymmetric configurations. Convergence effects in the external inviscid flow are important, except at very high Mach numbers.

2) The use of two-dimensional external flow relations in axisymmetric interaction calculations is therefore generally inadequate.

3) A method for calculating interactions on hollow cylinder-flare bodies at zero incidence, which uses the Lees-Reeves-Klineberg[6,9] boundary-layer method in axisymmetric form, in conjunction with an inversion of the second-order shock-expansion inviscid flow method of Syvertson and Dennis,[17] has been shown to yield results in excellent agreement with experiment when the extent of separated flow is not too large.

4) Differences between theory and experiment in the free-interaction region occur when the separated region is large, which may be attributed to inaccuracies in the basic Lees-Reeves-Klineberg method.

References

[1] Ackeret, J. et al., "Investigations of Compression Shocks and Boundary Layers in Gases Moving at High Speed," TM 1113, 1947, NACA.

[2] Liepmann, H. W., "The Interaction between Boundary Layer and Shock Waves in Transonic Flow," *Journal of the Aeronautical Sciences*, Vol. 13, No. 12, Dec. 1946.

[3] Chapman, D. R. et al., "Investigation of Separated Flows in Supersonic and Subsonic Streams with Emphasis on the Effect of Transition," Rept. 1356, 1958, NACA.

[4] Hakkinen, R. J. et al., "The Interaction of an Oblique Shock Wave with a Laminar Boundary Layer," Memo. 2-18-59W, 1959, NASA.

[5] Crocco, L. and Lees, L., "A Mixing Theory for the Interaction between Dissipative Flows and Nearly Isentropic Streams," *Journal of the Aeronautical Sciences*, Vol. 19, No. 10, Oct. 1952, pp. 649–676.

[6] Lees, L. and Reeves, B L., "Supersonic Separated and Reattaching Laminar Flows: I. General Theory and Application to Adiabatic Boundary-Layer/Shock-Wave Interactions," *AIAA Journal*, Vol. 2, No. 11, Nov. 1964, pp. 1907–1920.

[7] Nielsen, J. N. et al., "Calculation of Laminar Separation with Free Interaction by the Method of Integral Relations, Part I—Two-Dimensional Supersonic Adiabatic Flow," TR-65-107, Pt. I, 1965, Air Force Flight Dynamics Lab.

[8] Reyhner, T. and Flügge-Lotz, I., "The Interaction of a Shock Wave with a Laminar Boundary Layer," TR 163, 1966, Div. of Mechanical Engineering, Stanford Univ., Stanford, Calif.

[9] Klineberg, J. M. and Lees, L., "Theory of Laminar Viscous-Inviscid Interactions in Supersonic Flow," *AIAA Journal*, Vol. 7, No. 12, Dec. 1969, pp. 2211–2221.

[10] Kuehn, D. M., "Laminar Boundary-Layer Separation Induced by Flares on Cylinders at Zero Angle of Attack," TR R-146, 1962, NASA.

[11] Gray, J. D., "Laminar Boundary-Layer Separation on Flared Bodies at Supersonic and Hypersonic Speeds," TDR-64-277, 1965, Arnold Engineering Development Center.

[12] Kuehn, D. M. and Monson, D. J., "Boundary-Layer Separation and Reattachment With and Without Ablation," *Proceedings of the Specialists' Meeting on Separated Flows*, C.P. 4, Pt. I, 1966, pp. 121–145, AGARD.

[13] Ginoux, J. J., "Supersonic Separated Flows over Wedges and Flares with Emphasis on a Method of Detecting Transition," TN47, 1968, von Kármán Inst. for Fluid Dynamics, Rhode-Saint-Genèse, Belgium.

[14] Leblanc, R. and Ginoux, J. J., "Influence of Cross-flow on Two-dimensional Separation," TN 62, 1970, von Kármán Inst. for Fluid Dynamics, Rhode-Saint-Genèse, Belgium.

[15] Klineberg, J. M., "Theory of Laminar Viscous-Inviscid Interactions in Supersonic Flow," Ph.D. thesis, 1968, California Inst. of Technology, Pasadena, Calif.

[16] Nielsen, J. N. et al., "Calculation of Laminar Separation with Free Interaction by the Method of Integral Relations, Part II—Two-dimensional Supersonic Nonadiabatic Flow and Axisymmetric Supersonic Adiabatic and Nonadiabatic Flows," TR-65-107, Pt. II, 1966, Air Force Flight Dynamics Lab.

[17] Syvertson, C. A. and Dennis, D. H., "A Second-order Shock-expansion Method Applicable to Bodies of Revolution Near Zero Lift," Rept. 1328, 1957, NACA.

[18] Horton, H. P., "The Calculation of Adiabatic Laminar Boundary Layer Shock Wave Interactions in Axi-symmetric Flow: Part I. Hollow Cylinder-Flare Bodies with Zero Spin," TN 63, 1970, von Kármán Inst. for Fluid Dynamics, Rhode-Saint Genèse, Belgium.

[19] Stewartson, K., "Correlated Incompressible and Compressible Boundary Layers," *Proceedings of the Royal Society (London), Ser. A*, Vol. 200, No. A1060, 1949, pp. 84–100.

[20] Mangler, W., "Zusammenhang zwischen ebenen und rotations-symmetrischen Grenzschichten in kompressiblen Flüssigkeiten," *Zeitscrift fuer Angewandte Mathematik und Mechanik*, Vol. 28, 1948, pp. 97–103.

[21] Van Dyke, M. D., "Practical Calculation of Second-order, Supersonic Flow Past Nonlifting Bodies of Revolution," TN 2744, 1952, NACA.

[22] Ko, D. R. S. and Kubota, T., "Supersonic Laminar Boundary Layer along a Two-dimensional Adiabatic Curved Ramp," *AIAA Journal*, Vol. 7, No. 2, Feb. 1969, pp. 298–304.

[23] Riethmuller, M. L. and Ginoux, J. J., "A Parametric Study of Adiabatic Laminar Boundary Layer-Shock Wave Interactions by the Method of Lees-Reeves-Klineberg," TN 60, 1970, von Kármán Inst. for Fluid Dynamics, Rhode-Saint-Genèse, Belgium.

[24] Lewis, J. E. et al., "Experimental Investigation of Supersonic Laminar, Two-Dimensional Boundary-Layer Separation on a Compression Corner With and Without Cooling," *AIAA Journal*, Vol. 6, No. 1, Jan. 1968, pp. 7–14.

[25] Eggers, A. J., Jr. and Savin, R. C., "A Unified Two-Dimensional Approach to the Calculation of Three-Dimensional Hypersonic Flows, with Application to Bodies of Revolution," Rept. 1249, 1955, NACA.

[26] Goodwin, F. K., Nielsen, J. N., and Lynes, L. L., "Inhibition of Flow Separation at High Speed, Vol. II—Calculation of Nonadiabatic Laminar Boundary Layers," AFFDL-TR-68-119, Vol. II, 1969, Air Force Flight Dynamics Lab.

[27] Kuhn, G. D., Goodwin, F. K., and Nielsen, J. N., "Prediction of Supersonic Laminar Flow Separation by the Method of Integral Relations with Free Interaction," AFFDL-TR-69-87, 1970, Air Force Flight Dynamics Lab.